MRI-based habitat radiomics combined with vision transformer for identifying vulnerable intracranial atherosclerotic plaques and predicting stroke events: a multicenter, retrospective study

Yu Gao,[a,b,g] Ziang Li,[b,g] Xiaoyang Zhai,[a] Gang Zhang,[a] Lan Zhang,[a] Tingting Huang,[a] Lin Han,[b] Jie Wang,[b] Ruifang Yan,[b] Yongdong Li,[d] HongLing Zhao,[e] Qiuyi Zhao,[f] Zhengqi Wei,[b] Beichen Xie,[b] Yancong Sun,[b] Jianhua Zhao,[c,**] and Hongkai Cui[b,c,*]

[a]Department of MRI Center, The First Affiliated Hospital of Henan University of Chinese Medicine, Zhengzhou, China
[b]Department of Radiology Center, The First Affiliated Hospital of Xinxiang Medical University, Xin Xiang, China
[c]Department of Neurology Center, The First Affiliated Hospital of Xinxiang Medical University, Xin Xiang, China
[d]Institute of Diagnostic and Interventional Radiology, Shanghai Sixth People's Hospital Affiliated to Shanghai Jiao Tong University School of Medicine, Shanghai, China
[e]Department of Neurology Center, Xinxiang Central Hospital, Xin Xiang, China
[f]The Second School of Clinical Medicine, ZhengZhou University, Zhengzhou, China

eClinicalMedicine
2025;82: 103186

Published Online xxx
https://doi.org/10.1016/j.eclinm.2025.103186

Summary

Background Accurate identification of high-risk vulnerable plaques and assessment of stroke risk are crucial for clinical decision-making, yet reliable non-invasive predictive tools are currently lacking. This study aimed to develop an artificial intelligence model based on high-resolution vessel wall imaging (HR-VWI) to assist in the identification of vulnerable plaques and prediction of stroke recurrence risk in patients with symptomatic intracranial atherosclerotic stenosis (sICAS).

Methods Between June 2018 and June 2024, a retrospective collection of HR-VWI images from 1806 plaques in 726 sICAS patients across four medical institutions was conducted. K-means clustering was applied to the T1-weighted imaging (T1WI) and T1-weighted imaging with contrast enhancement (T1CE) sequences. Following feature extraction and selection, radiomic models and habitat models were constructed. Additionally, the Vision Transformer (ViT) architecture was utilized for HR-VWI image analysis to build a deep learning model. A stacking fusion strategy was employed to integrate the habitat model and ViT model, enabling effective identification of high-risk vulnerable plaques in the intracranial region and prediction of stroke recurrence risk. Model performance was evaluated using receiver operating characteristic (ROC) curves, and model comparisons were conducted using the DeLong test. Furthermore, decision curve analysis and calibration curves were utilized to assess the practicality and clinical value of the model.

Findings The fused Habitat + ViT model exhibited excellent performance in both the validation and test sets. In the validation set, the model achieved an area under the curve (AUC) of 0.949 (95% CI: 0.927–0.969), with a sensitivity of 0.879 (95% CI: 0.840–0.945), a specificity of 0.905 (95% CI: 0.842–0.949), and an accuracy of 0.897 (95% CI: 0.870–0.926). In the test set, the AUC increased to 0.960 (95% CI: 0.941–0.973), with specificity rising to 0.963 and an accuracy of 0.885 (95% CI: 0.857–0.913). The DeLong test revealed statistically significant differences in AUC between the fused model and the single-modal models (test set, vs. ViT $p = 0.000$; vs. Habitat $p = 0.000$) Cox regression analysis showed that the Habitat + ViT index, based on the prediction probability of the Habitat + ViT model, was an independent predictor of stroke recurrence (HR: 2.07; 95% CI: 1.12–3.81), with significant predictive power for stroke events at multiple time points. Specifically, measured by AUC values, the model's predictive performance at 1, 2, 3, and 4 years was 0.751 (95% CI: 0.679–0.823), 0.820 (95% CI: 0.760–0.876), 0.815 (95% CI: 0.753–0.877), and 0.780 (95% CI: 0.680–0.873), respectively.

Interpretation The integrated Habitat + ViT model based on HR-VWI demonstrated superior performance in identifying high-risk vulnerable plaques in sICAS patients and predicting stroke recurrence risk, providing valuable support for clinical decision-making.

*Corresponding author. Department of Neurology Center, The First Affiliated Hospital of Xinxiang Medical University, Xin Xiang, China.
**Corresponding author.
E-mail addresses: chk-1980@163.com (H. Cui), 051092@xxmu.edu.cn (J. Zhao).
[g]These authors have contributed equally to this work and share first authorship.

Funding This study was supported by the National Natural Science Foundation of China (grant 82204933). Henan Key Laboratory of Neurorestoratology (HNSJXF-2021-004), 2019 Joint Construction Project of Henan Provincial Health Committee and Ministry of Health (SB201901061), and the Xin Xiang City Acute Ischemic Stroke Precision Prevention and Treatment Key Laboratory.

Keywords: Habitat; Vision transformer; High-risk plaque; Stroke

Research in context

Evidence before this study

We conducted a literature search on Google Scholar and PubMed up to July 30, 2024, using the terms "(intracranial atherosclerotic plaque or vulnerable plaque) AND (habitat or heterogeneity) AND (prediction) AND (radiomics or deep learning)" without any language restrictions. However, current research primarily relies on traditional imaging techniques such as MRI and CT scans. Although high-resolution vessel wall imaging (HR-VWI) has enhanced plaque visualization, its diagnostic accuracy remains limited by subjective interpretation and incomplete capture of micro environmental features. Radiomics analysis, although applied in intracranial plaque studies, often treats plaques as homogeneous entities, neglecting spatial heterogeneity and dynamic interactions between subregions. Furthermore, deep learning techniques such as Vision Transformers (ViT) have shown promising prospects in plaque segmentation and stenosis rate identification. Yet, this is insufficient to meet the clinical needs for accurate vulnerability classification of plaques and prediction of long-term stroke recurrence risk in patients with sICAS (symptomatic intracranial atherosclerotic stenosis).

Added value of this study

To our knowledge, this is the first large-scale multicenter study to develop an integrated Habitat Radiomics and Vision Transformer (ViT) model using HR-VWI for identifying vulnerable intracranial plaques and predicting stroke recurrence. By combining K-means clustering to capture intraplaque heterogeneity and ViT's self-attention mechanism to analyze cross-regional interactions, our model achieved superior performance (AUC: 0.960 in the test set), significantly outperforming traditional radiomics and standalone ViT models. Notably, the Habitat + ViT index emerged as an independent predictor of stroke recurrence (HR: 2.07), with robust prognostic stratification across 1–4 years (AUC: 0.751–0.820). The model's interpretability highlighted critical features such as intraplaque hemorrhage and neovascularization, aligning with pathological mechanisms of plaque instability.

Implications of all the available evidence

Our findings demonstrate that integrating habitat radiomics with ViT enhances the precision of vulnerable plaque identification and stroke risk prediction, offering a non-invasive tool to guide clinical decision-making. The model's ability to quantify spatial heterogeneity and subregional interactions bridges a critical gap in current imaging analysis, enabling early intervention for high-risk patients. Future prospective studies should validate its utility in diverse populations and explore integration with multimodal imaging to further improve predictive accuracy. This approach holds promise for advancing personalized stroke prevention strategies in intracranial atherosclerosis.

Introduction

In recent years, with the rapid advancement of medical technology, prevention strategies for intracranial atherosclerotic stroke have achieved remarkable success. However, acute ischemic stroke (AIS) continues to rank among the top causes of morbidity and mortality globally, posing a significant threat to human health.[1,2] Medical imaging studies have revealed that AIS cases are often attributed to the instability of atherosclerotic plaques.[3–5] Therefore, early and precise identification of these high-risk vulnerable plaques is crucial for guiding clinical interventions and improving patient outcomes.

Intravascular ultrasound (IVUS) has demonstrated significant value in the analysis of coronary plaques; however, its application in intracranial arteries is constrained by technical hurdles, namely, the fragility of catheters in tortuous vessels and the associated high costs.[6] In comparison, high-resolution vessel wall imaging (HR-VWI) serves as a non-invasive assessment tool that combines high spatial resolution with the absence of ionizing radiation, enabling precise elucidation of the morphological features and tissue composition of intracranial plaques.[7,8] However, the completeness of plaque information provided by HR-VWI is highly reliant on the neuroimaging expertise of the radiologist. Radiomics has emerged as a pivotal approach to address this gap by extracting high-throughput imaging features to quantitatively characterize lesion morphology and composition.[9] Nevertheless, traditional radiomic methods often analyze plaques as homogeneous entities, failing to effectively capture their internal heterogeneity.[10] This technical bottleneck has been overcome in oncology

research through the innovative concept of "habitat imaging". This technological framework originates from the theory of tumor subregion analysis, employing unsupervised clustering algorithms to divide lesions into voxel clusters with similar imaging features (such as textural heterogeneity and signal intensity distribution). By accurately capturing internal variations within the lesion (such as tumor edema and necrosis), it effectively addresses the shortcomings of traditional radiomics.[11]

Concurrently, deep learning has revolutionized medical image analysis, with transformer architectures emerging as potent tools.[12] Unlike convolutional neural networks (CNNs), Vision Transformer (ViT) leverage a self-attention mechanism to establish dynamic weighted associations among lesions, capturing long-range dependencies across different regions.[13,14] This capability is crucial for analyzing pathological interactions between different habitats, such as inflammatory cell infiltrates, which are often overlooked by traditional and habitat-based radiomics approaches. The Transformer model has demonstrated promising applications in brain age estimation and intracranial vessel segmentation,[15–17] and it also exhibits significant advantages in plaque analysis. Specifically, studies have shown that the Transformer model outperforms traditional Convolutional Neural Networks in predicting coronary artery plaque erosion (AUC: 0.94 vs. 0.88). These findings underscore the Transformer's ability to integrate cross-regional information, which constitutes a key advantage in analyzing complex intracranial plaques.[18]

Based on these research advancements, we propose a hypothesis: The application of Habitat Radiomics to the analysis of atherosclerotic plaques allows for a more precise assessment of their unique pathological microenvironments, including intraplaque hemorrhage zones, neovascularization-dense areas, and stable fibrous matrix regions. By quantifying the specific biological processes within these subregions, we effectively address the common issue of spatial averaging in traditional radiomics. Furthermore, by integrating ViT technology, we are able to further uncover the long-term dependencies and interaction mechanisms among different subregions within plaques, thereby achieving a more comprehensive understanding of plaque information.

Therefore, the primary objective of this study is to develop and validate an integrated model based on ViT and Habitat Radiomics, utilizing HR-VWI of plaques, for the early and accurate identification of vulnerable plaques, and subsequently, for effective prediction of stroke recurrence risk.

Methods

Ethics statement

The study was approved by the Ethics Committee of The First Affiliated Hospital of Xinxiang Medical University (No.EC-022-142). As this was a retrospective study, the requirement for informedconsent was waived.

Patients

The study enrolled patients with symptomatic intracranial atherosclerotic stenosis (sICAS) between June 2018 and June 2024. For detailed inclusion and exclusion criteria, please refer to the Supplementary Appendix 1.

A total of 726 patients with sICAS from four centers were ultimately enrolled, yielding 1806 intracranial atherosclerotic plaques. Specifically, 400 patients from Center 1 (The First Affiliated Hospital of Xinxiang Medical University) comprised the training set, 158 patients from Center 2 (The First Affiliated Hospital of Henan University of Chinese Medicine) and Center 3 (Xinxiang Central Hospital) collectively formed the internal validation set, and 168 patients from Center 4 (The Sixth People's Hospital of Shanghai Jiao Tong University) served as the test set. The patient inclusion process is seen in Fig. 1. The overall study design is depicted in Fig. 2.

Image acquisition and preprocessing

Imaging data were acquired using four different magnetic resonance imaging (MRI) machines from four centers: the Ingenia Elition (Philips Medical Systems, Best, Netherlands), Ingenia CX (Philips Medical Systems, Best, Netherlands), MAGNETOM Vida (Siemens Healthineers, BioMatrix System, Germany), and Discovery MR750 (General Electric Company, America). A 3D high-resolution black-blood T1-weighted fast spin-echo sequence was employed, with the scanning area encompassing intracranial vessels of interest. Enhanced T1-weighted images were obtained following the administration of 0.1 mmol/kg of gadobutrol. Intracranial arterial stenosis was localized using 3D-TOF MRA. The total MRI scan duration ranged from 15 to 20 min, specific scan parameters and image preprocess detailed in the Supplementary Appendix 2. The inter-observer and intra-observer consistency assessments for image quality can be found in Supplementary Tables S1 and S2.

Plaque analysis

For plaque traditional characteristic analysis, the software TS-Vessel·Explore (TS imaging; Healthcare China, Beijing) was utilized. The specific operational procedures, definitions and criterias for plaque feature identification and assessment are provided in the Supplementary Appendix 3. The inter-observer and intra-observer consistency assessments for culprit plaques can be found in Supplementary Tables S3 and S4.

Follow-up and the definition of stroke recurrence

The follow-up for this study was primarily conducted through telephone interviews and reviews of medical

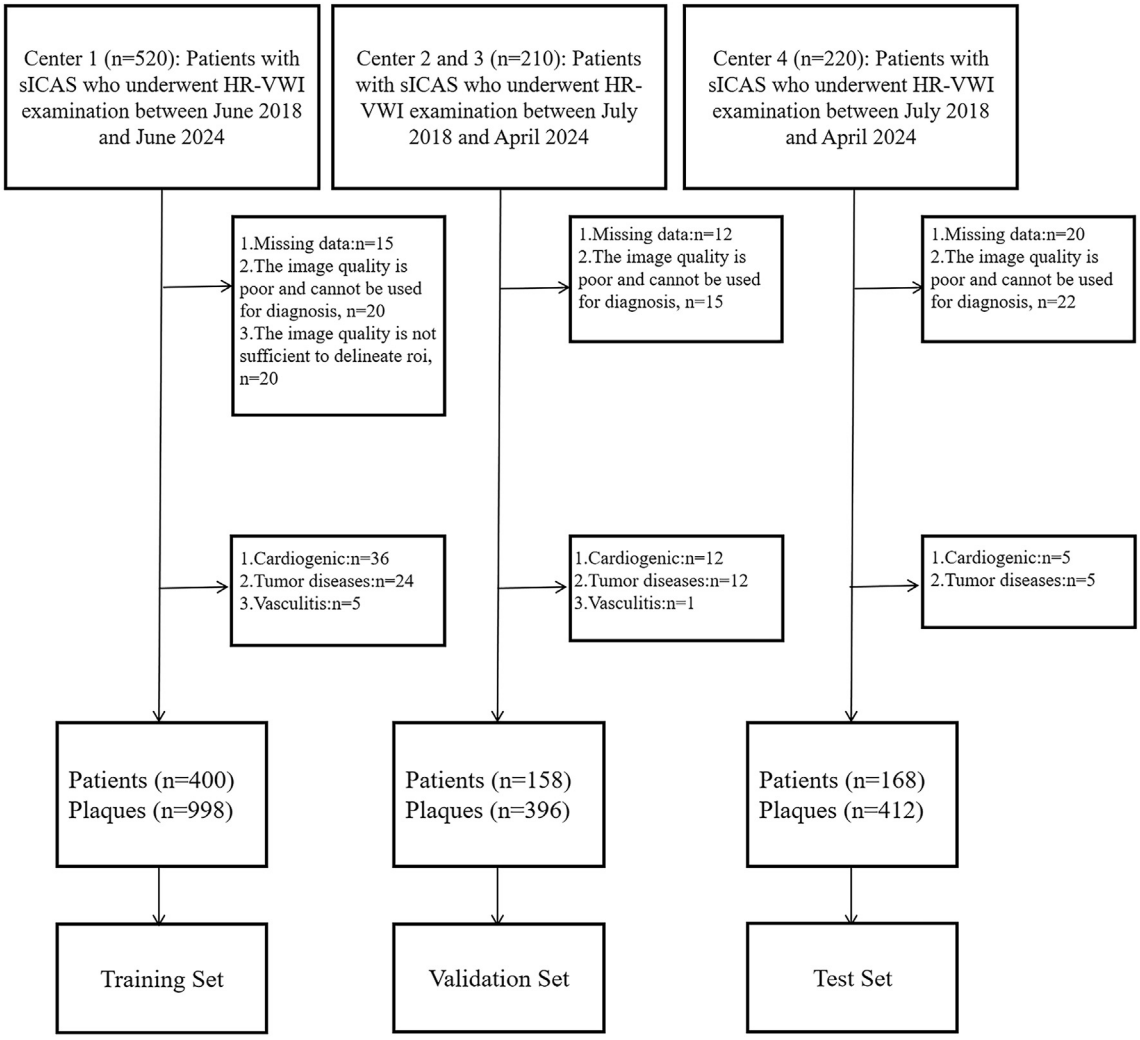

Fig. 1: Flow chart shows the patient inclusion exclusion of the three datasets. Center 1: The First Affiliated Hospital of Xinxiang Medical College, Center 2: Xinxiang Central Hospital, Center 3: The First Affiliated Hospital of Henan University of Traditional Chinese Medicine, Center 4: The Sixth People's Hospital of Shanghai Jiao Tong University.

record systems, with a follow-up duration ranging from 24 to 48 months and a median follow-up time of 37 months. All patients with complete follow-up information should undergo at least one comprehensive examination process, which includes a neurological examination, routine laboratory tests, and a cranial MRI scan. The diagnostic criteria for stroke recurrence include: (1) sudden onset of new focal neurological dysfunction lasting for more than 24 h. (2) Focal neurological dysfunction lasting less than 24 h but confirmed as acute cerebral infarction by imaging. (3) Sudden neurological deterioration with an increase of ≥4 points on the National Institutes of Health Stroke Scale (NIHSS) score.

ROI segmentation and habitats generation

The delineation of regions of interest (ROIs) for plaque analysis was based on both T1 and T1-contrast-enhanced (T1CE) sequences. The plaques and corresponding vascular layers were traced slice-by-slice, ensuring that tissues outside the vessel and plaque were excluded from the delineation. Randomly selecting 100 images, the study evaluated the consistency in delineating plaque ROI among radiology physicians of varying experience levels from four hospitals (Supplementary Table S5), as well as the intra-observer consistency of the same physician at different time points (with a 10-day interval) (Supplementary Table S6), all under the condition of being blinded to

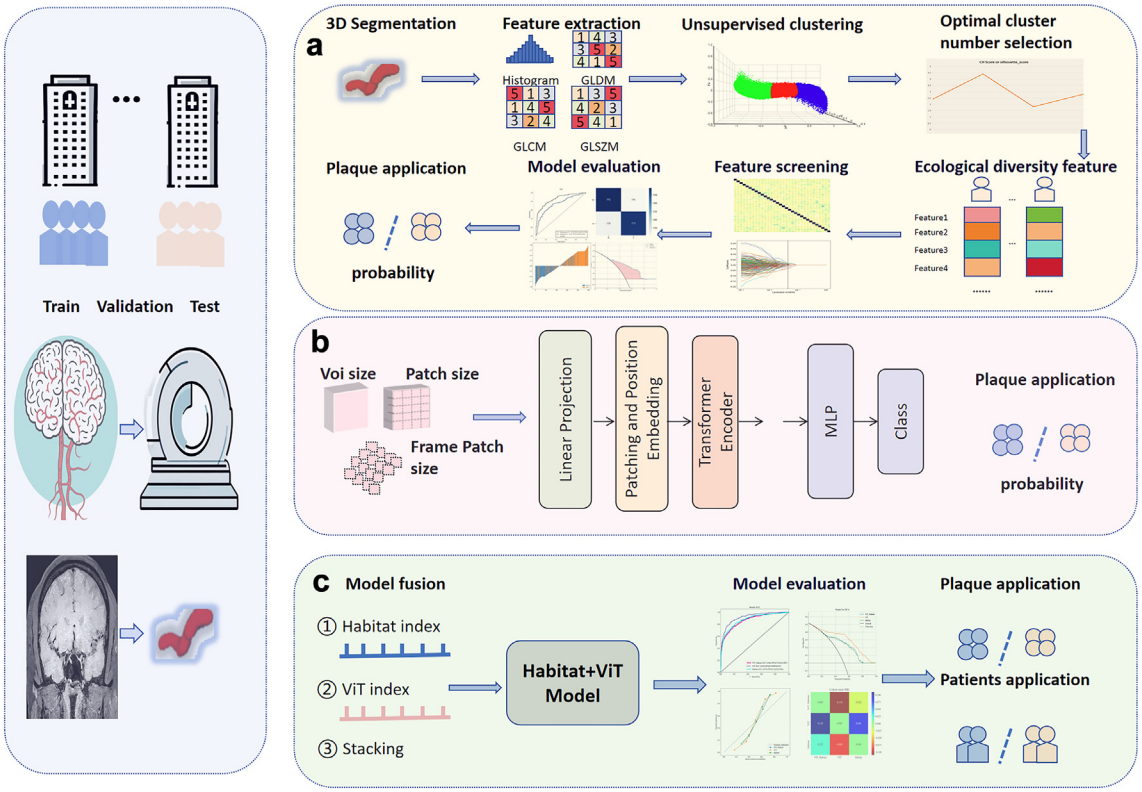

Fig. 2: The schematic diagram illustrates the workflow of the Habitat + ViT evaluation method used in this study. (a) Firstly, relevant imaging features are extracted from the manually delineated vascular regions involved by the plaque. Optimal cluster numbers are selected using K-means clustering to establish the Habitat model, which outputs the prediction probability of the plaque being vulnerable based on Habitat. (b) Secondly, the smallest bounding cube encompassing each plaque-affected vessel is input, and this three-dimensional cube is sliced into multiple patches through Patch and Frame Patch processes. These patches undergo linear transformation and positional encoding, followed by multi-head self-attention calculations. This process enables the model to focus on different regions of the feature map simultaneously, while positional encoding retains spatial information. A Multi-Layer Perceptron (MLP) is used to decode and fuse the information, outputting the prediction probability of the plaque being vulnerable based on ViT. (c) Finally, Stacking is employed for the post-fusion of Habitat and ViT, resulting in a new model called Habitat + ViT. This new model is used to re-predict plaque vulnerability, and the Habitat + ViT index is utilized to stratify the risk of stroke recurrence in patients.

the clinical outcomes. The Dice Similarity Coefficient was used as the evaluation criterion to ensure the accuracy and reliability of plaque ROI delineation.

Features were extracted from each voxel within the volume of interest (VOI), including first-order features and textural features such as the Gray-Level Size Zone Matrix (GLSZM), Gray-Level Co-occurrence Matrix (GLCM), Neighborhood Gray-Tone Difference Matrix (NGTDM), Gray-Level Dependence Matrix (GLDM), and Gray-Level Run-Length Matrix (GLRLM). K-means clustering was performed separately on T1 and T1CE images using the scikit-learn Python package. Cluster numbers ranging from 2 to 9 were tested, and the optimal cluster number was selected based on the Calinski-Harabasz index and silhouette coefficient. After clustering, subregions sharing the same cluster ID were merged to form comprehensive habitat regions, each representing distinct microenvironmental features within the ROI. Detailed clustering procedures and the selection of the optimal cluster number are provided in the Supplementary Appendix 4. In this study, the optimal cluster number was determined to be 3 for both T1 and T1CE sequences (Supplementary Fig. S1).

Feature extraction selection, and habitat model construction

Features were extracted from the regions delineated on T1WI and T1CE sequence images. For each subregion, 108 radiomic features were extracted using the Pyradiomics Python package (version 3.0.1). All features extracted from the ROIs were normalized and standardized using the Z-score normalization method, and Habitat features were integrated by combining features

from different subregions. The calculation formula is as follows:

$$\text{Habitat Feature} = \text{Habitat}_1\ \text{Feature} + \text{Habitat}_2\ \text{Feature} + \text{Habitat}_3\ \text{Feature}$$

Feature Selection: (1) The Mann–Whitney U test was performed, and only features with $p < 0.05$ were retained. (2) Pearson correlation coefficients were calculated, and in cases where the correlation exceeded a threshold of 0.9, only one feature was retained from each pair of highly correlated features. (3) The Least Absolute Shrinkage and Selection Operator (LASSO) with 10-fold cross-validation was utilized to select the final set of features.

The final Habitat radiomic features were input into a support vector machine (SVM) machine learning classifier to construct separate radiomic feature models for T1 and T1CE.

Construction of radiomics model

Radiomic features extracted from the entire ROI were utilized to develop the Radiomics Model. The same feature selection and model construction procedures were applied to establish the Radiomics Model.

In this study, we have developed a vulnerable plaque classifier based on ViT. The model comprises six transformer blocks for extracting spatially dependent features of plaques, as well as an MLP Head classification layer to obtain classification results for predicting vulnerable plaques. This network takes plaque VOIs as input and generates outputs in the form of probability values to classify the plaques. Specific details regarding the construction of the ViT model and its training parameters can be found in Supplementary Appendix 5 and Fig. S2.

The fusion of models

Both model fusion between two sequences and fusion across models employing diverse techniques utilize the stacking ensemble method. Stacking, an ensemble learning technique, integrates the outputs (prediction probabilities) of multiple models using a meta-classifier to produce a single predictive outcome, thereby generating a post-fusion model.

Statistical analysis

All statistical analyses were conducted using R and Python. Continuous data that followed a normal distribution were expressed as mean ± standard deviation ($\bar{x} \pm s$), whereas non-normally distributed continuous data were presented as median (interquartile range) [M (P25, P75)]. Categorical data were reported in terms of counts and percentages. Univariable and multivariable Cox regression analyses were performed to screen for risk variables. The ROC curve was utilized to assess predictive performance, and the DeLong test was applied to compare differences in AUC among various models. p-value < 0.05 was considered statistically significant. We define the research on vulnerable plaque identification as Study 1 and the study on stroke recurrence prediction as Study 2. The detailed statistical methods for both Study 1 and Study 2 are provided in the Supplementary Appendix 6.

Role of the funding source

The funding sources played no role in the study design, data collection, data analysis, data interpretation, or writing of the manuscript.

Results

Patients data

The training group, the validation group, and the patients included in the test group were not statistically significant in terms of the clinical baseline data (Table 1) ($p > 0.05$).

Habitat clustering, feature extraction and selection

The optimal number of clusters was determined based on the Calinski-Harabasz (CH) index and silhouette score, with a gradual decline observed after three clusters (Supplementary Fig. S1). Consistently, the best clustering number for both T1 and T1CE sequences in this study was identified as three. Fig. 3 illustrates the clustering results for both T1 and T1CE sequences from the same patient, where Habitat 1 and Habitat 2 represent the remaining vascular lumen and thickened vascular wall (plaque), respectively, and Habitat 3 mainly represents T1-hyperintense components within the plaque in T1WI and enhanced components within the plaque in T1CE. Radiomic features were extracted from the three subregions of both T1WI and T1CE sequences, yielding a total of 273 features. Lasso regression was employed to select the most relevant features from each habitat subregion for inclusion in the final model. Specifically, 17 features were selected from T1WI, with 6 from Habitat 1, 5 from Habitat 2, and 6 from Habitat 3. For T1CE, 34 features were selected, including 14 from Habitat 1, 5 from Habitat 2, and 15 from Habitat 3 (Supplementary Fig. S3).

T1, T1CE and the stacking model efficacy comparison

In our study of Radiomics, Habitat, and ViT models, we employed a stacking approach to fuse dual-sequence models and evaluated their performance across three cohorts. The results demonstrated that the fused dual-sequence model outperformed single-sequence models. In the test set, the radiomics model achieved an AUC of 0.748 (95% CI: 0.697–0.795), sensitivity of 0.733 (95% CI: 0.498–0.797), specificity of 0.673 (95% CI: 0.627–0.892), and accuracy of 0.716 (95% CI: 0.675–0.755) (Supplementary Table S7). In comparison,

Variables	ALL (n = 726)	Training set (n = 400)	Validation set (n = 158)	Test set (n = 168)	p
Sex, n (%)					
Male	492 (67.8)	269 (67.3)	110 (69.6)	113 (67.3)	0.853
Female	234 (32.2)	131 (32.8)	48 (30.4)	55 (32.7)	
Age, median (IQR)	58.0 (51.0,66.0)	58.0 (51.0,66.0)	59.0 (51.0,66.0)	58.0 (51.0,66.0)	0.954
Smoke, n (%)					
No	418 (57.6)	230 (57.5)	87 (55.1)	101 (60.1)	0.652
Yes	308 (42.4)	170 (42.5)	71 (44.9)	67 (39.9)	
Drink, n (%)					
No	502 (69.1)	276 (69.0)	102 (64.6)	124 (73.8)	0.194
Yes	224 (30.9)	124 (31.0)	56 (35.4)	44 (26.2)	
Hypertension, n (%)					
No	294 (40.5)	161 (40.3)	61 (38.6)	72 (42.9)	0.729
Yes	432 (59.5)	239 (59.8)	97 (61.4)	96 (57.1)	
Diabetes, n (%)					
No	530 (73.0)	290 (72.5)	120 (75.9)	120 (71.4)	0.619
Yes	196 (27.0)	110 (27.5)	38 (24.1)	48 (28.6)	
TC, median (IQR)	4.0 (3.3,4.7)	4.0 (3.3,4.6)	4.0 (3.3,4.6)	4.0 (3.3,4.7)	0.816
TG, median (IQR)	1.2 (0.9,1.7)	1.2 (0.9,1.7)	1.2 (0.9,1.7)	1.3 (0.9,1.7)	0.967
LDL, median (IQR)	2.3 (1.8,2.8)	2.3 (1.8,2.8)	2.2 (1.8,2.8)	2.4 (1.7,2.9)	0.964
HDL, median (IQR)	1.1 (0.9,1.3)	1.1 (0.9,1.3)	1.1 (0.9,1.2)	1.1 (0.9,1.3)	0.770
ApoA, median (IQR)	1.1 (1.0,1.3)	1.1 (1.0,1.3)	1.1 (1.0,1.2)	1.1 (1.0,1.3)	0.786
ApoB, median (IQR)	0.8 (0.7,1.0)	0.8 (0.7,1.0)	0.8 (0.7,1.0)	0.8 (0.6,1.0)	0.741

TC, Total Cholesterol; TG, Triglyceride; LDL, Low-Density Lipoprotein; HDL, High-Density Lipoprotein.

Table 1: **Clinical characteristics of the training set, validation set and test set.**

the Habitat model exhibited improved performance with an AUC of 0.857 (95% CI: 0.819–0.889), sensitivity of 0.692 (95% CI: 0.599–0.860), specificity of 0.866 (95% CI: 0.694–0.942), and accuracy of 0.789 (95% CI: 0.750–0.825) (Supplementary Table S8). Notably, the ViT model demonstrated superior predictive capability, with an AUC of 0.913 (95% CI: 0.882–0.939), sensitivity of 0.851 (95% CI: 0.714–0.914), specificity of 0.825 (95% CI: 0.762–0.953), and accuracy of 0.843 (95% CI: 0.811–0.877) (Supplementary Table S9).

Habitat and radiomics model comparison

In both the validation and test sets, we further compared the performance of the Habitat model with the radiomics model. The results showed that the Habitat model achieved improvements of 0.109 and 0.073 in AUC and accuracy, respectively, with a significant increase in specificity to 0.866 (Supplementary Fig. S4 and Table S10). The DeLong test indicated that the difference in AUC between the Habitat model and the radiomics model was statistically significant (p = 0.000) (Supplementary Table S11).

Habitat + ViT model construction and performance

Given the superior predictive performance of the ViT model in the test set, it was integrated with the Habitat model using a stacking approach. The fused model exhibited excellent performance in both the validation and test sets. In the validation set, it achieved an AUC of 0.949 (95% CI: 0.927–0.969), sensitivity of 0.879 (95% CI: 0.840–0.945), specificity of 0.905 (95% CI: 0.842–0.949), and accuracy of 0.897 (95% CI: 0.870–0.926). In the test set, the AUC was 0.960 (95% CI: 0.941–0.973), with specificity increasing to 0.963 and accuracy of 0.885 (95% CI: 0.857–0.913) (Fig. 4 and Table 2). The DeLong test confirmed that the differences in AUC between the fused model and the two individual models were statistically significant (test set, vs. ViT p = 0.000; vs. Habitat p = 0.000) (Supplementary Table S12). Additionally, positive values for both the Net Reclassification Improvement (NRI) and Integrated Discrimination Improvement (IDI) indices further validated the enhanced predictive capability of the fused model (validation set, vs. Habitat, NRI = 0.013, IDI = 0.001; vs. ViT, NRI = 0.199, IDI = 0.155; test set, vs. Habitat, NRI = 0.015, IDI = 0.006; vs. ViT, NRI = 0.132, IDI = 0.150) (Supplementary Fig. S5 and Table S13).

Calibration curve analysis demonstrated good agreement between the predicted probabilities of the Habitat + ViT model and the observed outcomes, indicating high reliability of the model's predictions. Furthermore, clinical decision curve analysis emphasized the potential value of the model in guiding clinical decision-making, as its curve characteristics showed that the model provided useful information across different thresholds, facilitating more rational and scientific decisions by clinicians (Fig. 5).

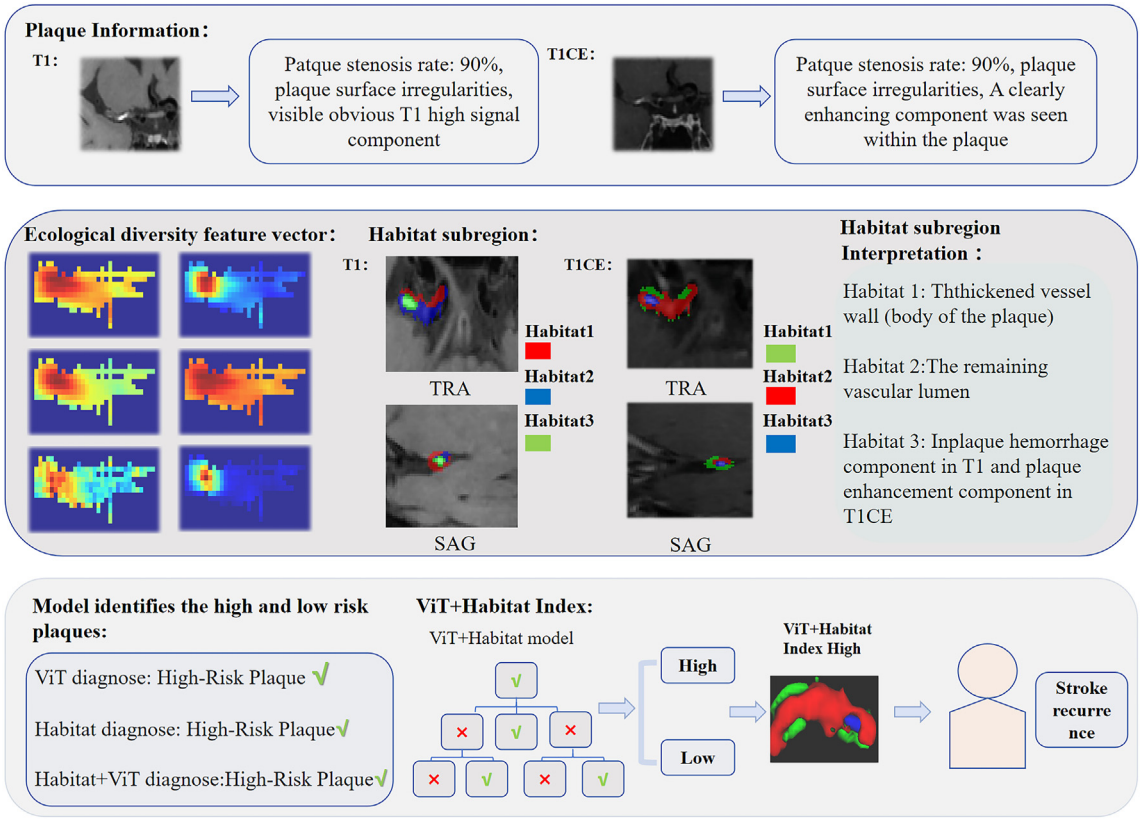

Fig. 3: The illustration depicts a 68-year-old male patient with sICAS. HR-VWI examination revealed a plaque in the M1 segment of the right middle cerebral artery, which was diagnosed as the culprit plaque. Imaging analysis showed that the patient had a stenosis rate of 93%, with an irregular plaque surface and a prominently high T1 signal, indicating intra-plaque hemorrhage. Additionally, the enhanced scan demonstrated significant enhancement of the plaque, suggesting a rich presence of neovascularization. Radiomics techniques were employed to extract plaque information, and unsupervised K-means clustering was utilized for categorization. The three Habitat regions provided a clear distinction among different components of the vessel and plaque. The culprit plaque in this patient was diagnosed as vulnerable by the Habitat model. Subsequent diagnoses using the ViT model and the Habitat + ViT model both confirmed the plaque as vulnerable. The Habitat + ViT index was utilized for risk stratification of stroke recurrence in the patient, yielding a score of 0.93, classifying him as high-risk. Follow-up results indicated that the patient experienced a recurrent stroke event at the 24-month mark.

Model prognostic assessment

Essential information

A total of 355 patients had complete follow-up information, among which 79 (22.2%) experienced stroke events. There were no statistically significant differences in baseline clinical characteristics between the stroke recurrence and non-recurrence groups ($p > 0.05$) (Supplementary Table S14). The predictive probability values from the traditional radiomics model, Habitat imaging model, ViT model, and the fused Habitat + ViT model were defined as the Radiomics index, Habitat index, ViT index, and Habitat + ViT index, respectively, with a range of 0–1.

Univariable and multivariable cox regression analyses

In the univariable Cox regression analysis, the Radiomics index, Habitat index, ViT index, and Habitat + ViT index emerged as risk factors for stroke recurrence, whereas traditional vulnerable plaque factors such as intraplaque hemorrhage (IPH) and low-attenuation plaque components with no calcification (LRNC) were not statistically significant. The multivariable Cox regression analysis revealed that the Habitat + ViT index was an independent risk factor for predicting stroke recurrence (HR: 2.07; 95% CI: 1.12, 3.81) (Table 3).

Incremental prognostic value of the habitat + ViT model

To accurately predict stroke recurrence events, we selected four univariate variables with positive predictive values. To evaluate the predictive performance of these variables, we employed time-dependent Receiver Operating Characteristic (Time-ROC) curves for analysis. Specifically, based on patients' HR-VWI data, we extracted four core parameters using the Habitat radiomics approach, traditional radiomics techniques, and the ViT model. These parameters were utilized to

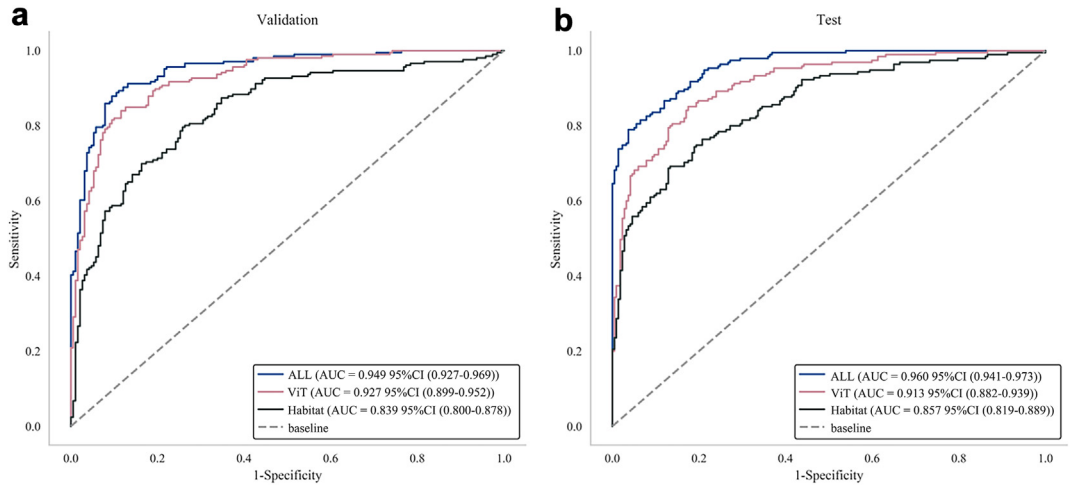

Fig. 4: Comparison of Receiver Operating Characteristic (ROC) curves for ViT model, Habitat model and Habitat + ViT in the Validation set (a) and Test set (b). The lower right corners of Figure (a) and Figure (b) respectively display the area under the curve and its 95% Confidence Interval for each model. All = Habitat + ViT.

predict the risk of stroke recurrence within 1, 2, 3, and 4 years for patients, respectively. The results demonstrated that the Habitat + ViT index exhibited the most prominent predictive ability for stroke events across multiple time points. Specifically, the model's predictive performance at 1, 2, 3, and 4 years, as measured by the AUC values, were 0.751 (95% CI: 0.679–0.823), 0.820 (95% CI: 0.760–0.876), 0.815 (95% CI: 0.753–0.877), and 0.780 (95% CI: 0.680–0.873), respectively (Fig. 6). Furthermore, patients were stratified into high-risk and low-risk groups based on the Habitat + ViT Index (using the ROC curve's cut-off value as the threshold). The Kaplan–Meier survival curves revealed a significant difference in the log-rank test ($p < 0.0001$), further validating the model's effectiveness in stroke risk stratification (Fig. 7).

Discussion

For patients with sICAS, accurate and timely assessment of intracranial plaque vulnerability is crucial for optimizing treatment strategies and improving clinical outcomes. In this multicenter study, we innovatively developed an integrated model, termed "Habitat + ViT". This model integrates HR-VWI technology, ViT algorithms, and Habitat Radiomics analysis to deeply explore plaque characteristic information. The research results indicate that this comprehensive model demonstrates extremely high predictive accuracy in identifying vulnerable plaques. More importantly, the model also exhibits exceptional predictive performance in assessing the risk of stroke recurrence among sICAS patients.

ICAS constitutes the core pathogenic mechanism of acute ischemic stroke.[19] Previous research has indicated

Model	AUC (95% CI)	Sensitivity (95% CI)	Specificity (95% CI)	Accuracy
Train				
ViT	0.916 (0.900–0.932)	0.838 (0.748–0.883)	0.850 (0.811–0.933)	0.846 (0.826–0.868)
Habitat	0.874 (0.854–0.895)	0.812 (0.667–0.851)	0.788 (0.753–0.912)	0.804 (0.780–0.826)
ViT + Habitat	0.953 (0.940–0.963)	0.870 (0.811–0.915)	0.892 (0.854–0.947)	0.884 (0.864–0.904)
Validation				
ViT	0.927 (0.899–0.952)	0.840 (0.775–0.932)	0.884 (0.796–0.945)	0.867 (0.833–0.896)
Habitat	0.839 (0.800–0.878)	0.796 (0.618–0.908)	0.742 (0.636–0.920)	0.779 (0.741–0.817)
ViT + Habitat	0.949 (0.927–0.969)	0.879 (0.840–0.945)	0.905 (0.842–0.949)	0.897 (0.870–0.926)
Test				
ViT	0.913 (0.882–0.939)	0.851 (0.714–0.914)	0.825 (0.762–0.953)	0.843 (0.811–0.877)
Habitat	0.857 (0.819–0.889)	0.692 (0.599–0.860)	0.866 (0.694–0.942)	0.789 (0.750–0.825)
ViT + Habitat	0.960 (0.941–0.973)	0.790 (0.764–0.972)	0.963 (0.778–0.982)	0.885 (0.857–0.913)

Table 2: **Comparing the performance of the three models in the training set, validation set and test set in predicting the performance of high-risk vulnerable plaques.**

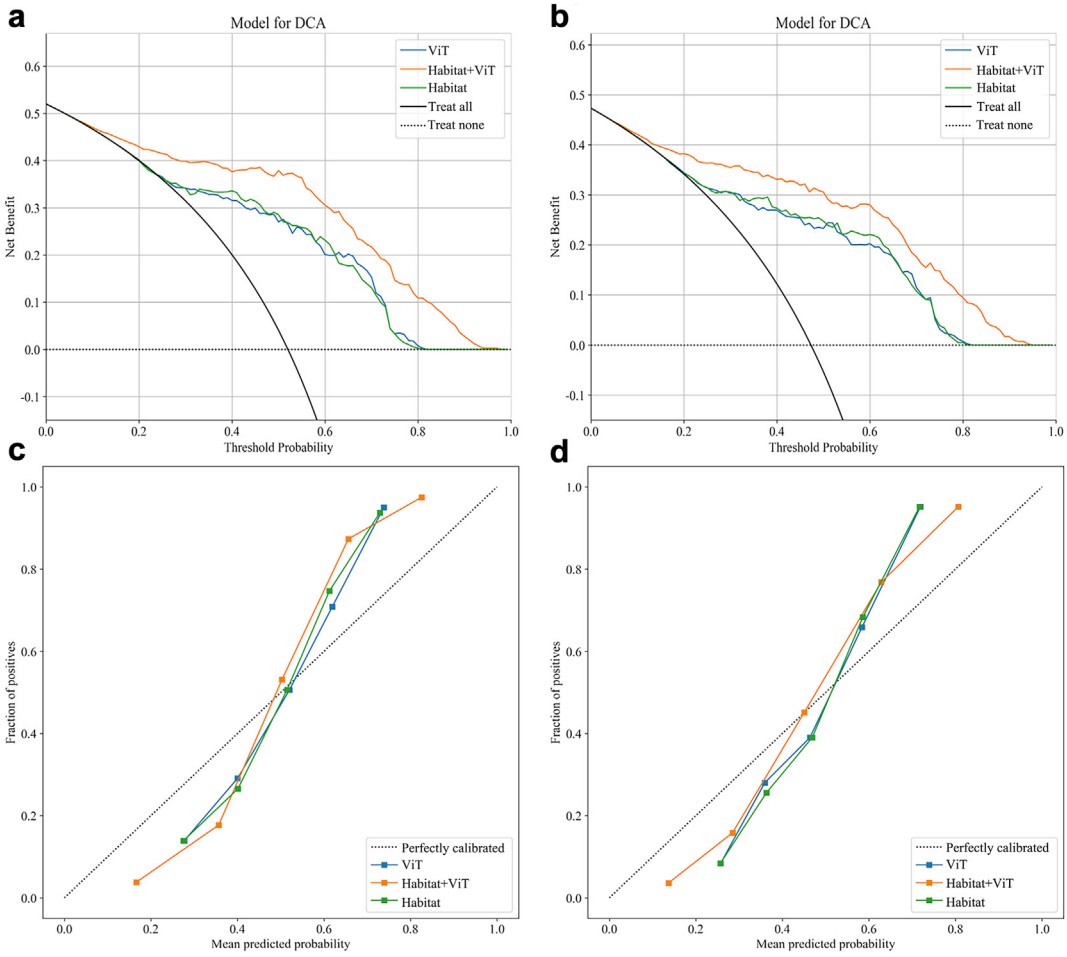

Fig. 5: Evaluation of Calibration Curves and Clinical Decision Curves for All Models in the Validation set (a and c) and Test set (b and d). (a, b) Clinical Decision Curve Analysis: This curve plots risk threshold on the x-axis and net benefit on the y-axis. Across a wide range of thresholds, the results demonstrate that the integrated Habitat + ViT model exhibits higher net benefit performance compared to the standalone Habitat and ViT models. (c, d) Calibration Curve Analysis: The x-axis represents the average predicted probability, while the y-axis represents the actual probability of event occurrence. The dashed line serves as a reference line indicating perfect calibration, and the solid lines depict the fit of different models. The closer the fit line is to the reference line, the higher the predictive accuracy of the model. The calibration curves in (c) and (d) show that the fit line of the integrated Habitat + ViT model is more evenly distributed around the reference line, indicating higher predictive accuracy compared to the standalone Habitat and ViT models.

that features such as plaque enhancement and intraplaque hemorrhage are risk factors for stroke recurrence.[20,21] The pathophysiological processes of plaques are complex and variable, leading to a high degree of heterogeneity in their internal structures. The diverse compositions and morphologies of plaques often result in different clinical outcomes, with plaques exhibiting high-risk characteristics typically classified as vulnerable plaques.[22] However, given the internal complexity of plaques, the assessment of vulnerable plaques largely depends on the subjective experience of seasoned neuroimaging experts, which may lead to incomplete acquisition of plaque information and subsequently exert adverse effects on clinical diagnosis and treatment.

As a branch of machine learning, radiomics, with its high-throughput image information extraction capabilities, has been widely applied in the field of medical imaging, partially addressing the issue of omitted information in complex lesion imaging.[23] A study applied this technology to intracranial atherosclerotic plaque research and confirmed the excellent performance of the T1/T1CE dual-sequence fusion model in plaque risk assessment (AUC = 0.903, accuracy = 0.851).[24] Although this study confirmed that the dual-sequence model outperforms the single-sequence model (test set AUC = 0.748, 95% CI: 0.697–0.795; accuracy = 0.716, 95% CI: 0.675–0.755), the performance of the model built based on multicenter/multidevice data was still

Variables	Univariable COX		Multivariable COX	
	HR (95% CI)	p	HR (95% CI)	p
ViT index	4.45 (2.72,7.29)	0.000	2.13 (0.99,4.60)	0.050
Radiomics index	4.11 (2.52,6.69)	0.000	1.60 (0.64,4.01)	0.317
Habitat index	4.13 (2.52,6.77)	0.000	1.48 (0.73,2.98)	0.278
ViT + Habitat index	5.18 (3.13,8.56)	0.000	2.07 (1.12,3.81)	0.020
IPH	1.50 (0.90,2.50)	0.121		
LRNC	1.52 (0.93,2.49)	0.098		
FC rupture	1.25 (0.78,2.00)	0.350		
Stenosis rate				
30%–50%				
51%–70%	1.07 (0.65, 1.76)	0.791		
71%–99%	0.86 (0.43, 1.70)	0.662		
Enhancement level				
0				
1	1.16 (0.60, 2.25)	0.655		
2	1.30 (0.62, 2.73)	0.497		
3	1.41 (0.71, 2.78)	0.338		
Culprit plaque				
MCA				
ACA	2.40 (0.57, 10.05)	0.231		
PCA	5.87 (1.79, 19.29)	0.004		
VBA	0.73 (0.46, 1.18)	0.205		
ICA	1.76 (0.73, 4.21)	0.202		

Table 3: **Results of univariable and multivariable cox proportional hazard regression analyses for determining predictors of stroke events.**

lower than expected. Compared to that study, the present research employed a larger-scale, multicenter dataset encompassing multiple imaging devices, thereby enhancing the reliability of the data. However, the predictive performance was relatively low, which may be attributed to the current radiomics techniques partly neglecting the intraplaque heterogeneity. In contrast to tumor lesions, plaques are smaller in size and more complex in composition. Traditional radiomics, based on the assumption of homogeneous distribution of imaging heterogeneity, analyzes plaques as uniform entities, leading to an inability to effectively capture spatial heterogeneity features of microstructures and consequently resulting in the loss of critical spatial location information.[10]

Habitat analysis effectively reveals internal heterogeneity by dividing lesion subregions, enhancing the comprehensive understanding of the lesion. This technology has been widely used in the field of oncology,[25] such as Liu's use of Gaussian mixture clustering combined with habitat radiomics to predict pathological complete response to neoadjuvant chemotherapy in breast cancer (AUC = 0.83).[26] Intracranial atherosclerotic plaques share some similarities with tumors, with differences in composition and spatial distribution corresponding to different risk levels. In this study, K-Means clustering was applied to determine an optimal cluster number of 3: Habitat 1 corresponds to vessel wall thickening (fibrous body of the plaque), Habitat 2 to residual lumen, and Habitat 3 shows intraplaque hemorrhage on T1 and enhancing components on T1CE. Such subregion division provides a clear display of high-risk signs of plaques. Compared to traditional radiomics, the AUC and accuracy of the habitat model increased by 0.109 and 0.073, respectively, with a specificity of 0.866, making up for the lack of spatial heterogeneity in traditional radiomics. However, the model showed limited performance in external validation (accuracy = 0.789, 95% CI: 0.750–0.825; sensitivity = 0.692), mainly due to the neglect of interactions between plaque subregions by subregion segmentation, which is particularly important in vulnerable plaques: for example, persistent inflammatory responses within vulnerable plaques can mediate interactions between inflammatory areas and the plaque surface, degrade the fibrous cap collagen, and promote rupture, while neovascularization exacerbates plaque instability through hemorrhage. Habitat analysis ignores such dynamic interactions, leading to decreased sensitivity and accuracy.

Transformer, as an emerging deep learning technology, learns the relationships between different parts of an image through its unique attention mechanism and is increasingly applied in medicine.[27] Liu developed an integrated model based on ViT for the segmentation of coronary artery calcified plaques in intravascular

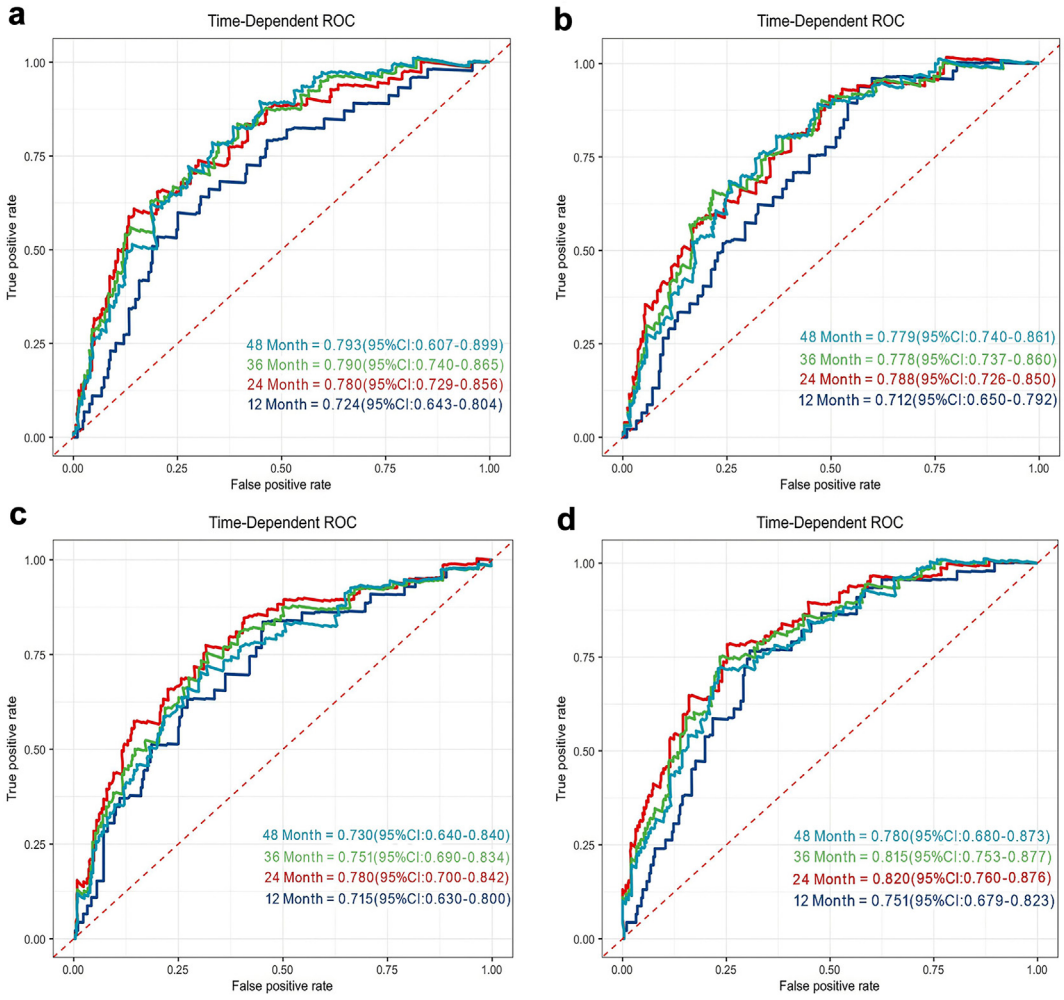

Fig. 6: Comparison of Time-dependent Receiver Operating Characteristic (ROC) curves for Radiomics Model (a), Habitat model (b), ViT model (c), and Habitat + ViT model (d). The lower right corners of Figures respectively display the area under the curve and its 95% Confidence Interval for each model.

optical coherence tomography images, achieving excellent performance, with the Dice value of 83.79%.[28] In this study, the ViT model also exhibited excellent performance, with an AUC value of 0.913 (95% CI: 0.882–0.939) in the test set, sensitivity of 0.851, specificity of 0.825, and accuracy of 0.843 (95% CI: 0.811–0.877). The model's excellent performance may be related to the attention mechanism of ViT, which enables the model to capture important relationships between various locations in the image, thereby better understanding the image content. Therefore, we believe that the attention mechanism of ViT can be utilized to compensate for the dynamic correlations between image regions, thereby improving the interrelationship between plaque features and local stability.

Consequently, we fully integrated the complex spatial heterogeneity within plaques and the information on interactions between various regions, ultimately fusing the Habitat model with the ViT model to obtain comprehensive imaging information of plaques. The Habitat + ViT model achieved the best performance in comparisons. This integration enabled the model to achieve excellent specificity (96.3%) by minimizing false positives for stable plaques while maintaining high sensitivity (79.0%) through integrated pattern recognition. The resulting AUC for the test set was 0.960, which not only outperformed the independent radiomics (AUC: 0.748) and ViT (AUC: 0.913) models but also demonstrated excellent generalization in multicenter datasets, emphasizing its robustness in different clinical settings. Additionally, univariate and multivariate Cox regression surprisingly showed that the Habitat + ViT index was an independent risk factor for stroke recurrence (HR: 2.07, 95% CI: 1.12, 3.81). Moreover, the

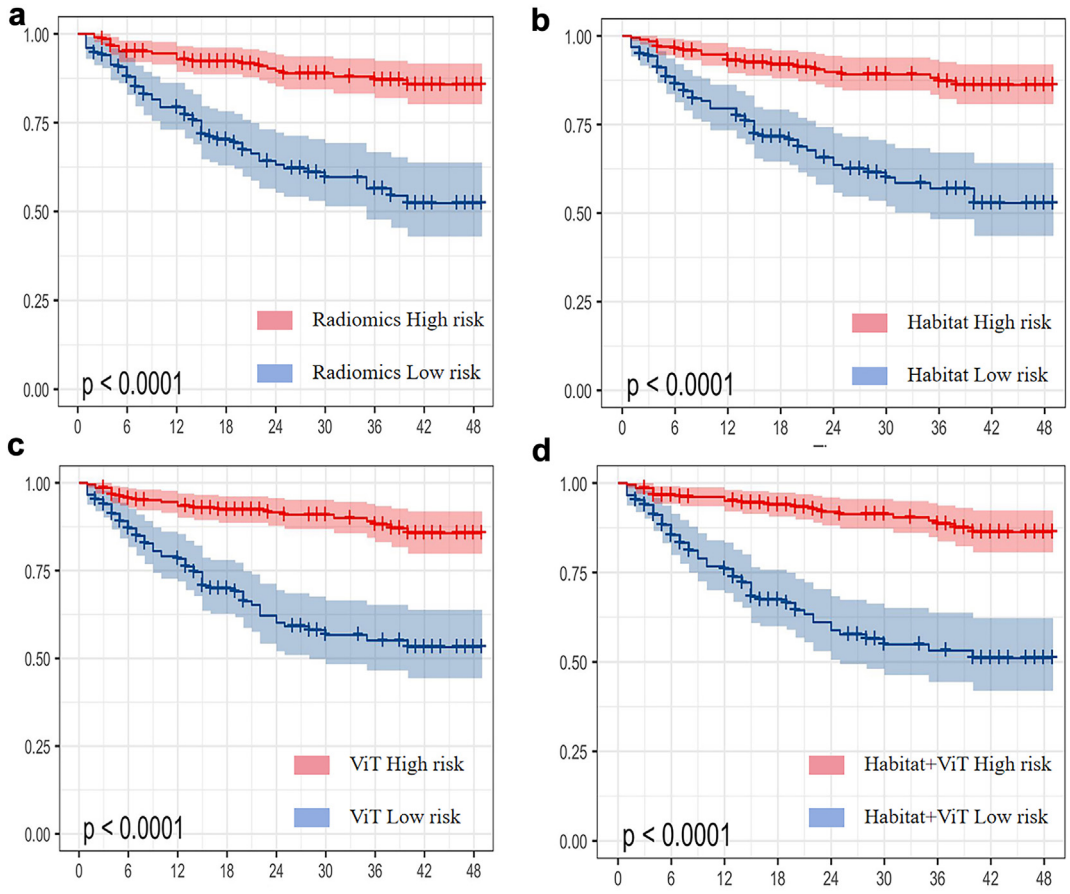

Fig. 7: The Kaplan–Meier curve stratified by high-risk and low risk factors by radiomics index (a), habitat index (b) ViT index (c) and habitat + ViT index (d).

model demonstrated certain effectiveness in stroke risk stratification (log-rank $p < 0.001$) and had good clinical value for predicting the risk of stroke recurrence: the AUC values at the 1-year, 2-year, 3-year, and 4-year time points were 0.751, 0.820, 0.815, and 0.780, respectively. This also aligns with the high correlation between vulnerable plaques and stroke events, with the model demonstrating high accuracy in plaque classification and thus having good predictive value for stroke recurrence events. Such a model has good clinical value for the qualitative diagnosis of plaques and early stroke risk stratification in sICAS patients for early intervention therapy. Fig. 3 shows the basic workflow of the model in clinical application. Case study: a 68-year-old male sICAS patient with three Habitat regions clearly delineating different components of the vessel and plaque. The patient had obvious plaque enhancement and intraplaque hemorrhage components. The patient's culprit plaque was diagnosed as vulnerable by the Habitat + ViT model. Based on the Habitat + ViT index (0.93), the patient was classified as high-risk for stroke recurrence. Follow-up results showed that the patient experienced a stroke recurrence event at 24 months. This indicates that the combination of the Habitat model and ViT model can more accurately analyze plaque image information, provide clear stroke risk stratification, and has good clinical potential.

However, this study has several limitations: (1) The retrospective design inherently introduces selection bias and unmeasured confounding factors, which may limit the generalization of the research results to a broader clinical population. Although external validation was conducted to improve reliability, prospective multicenter studies are still necessary for robust clinical translation. (2) Our imaging analysis was intentionally limited to T1 and T1CE sequences based on their established sensitivity in previous neurovascular studies for plaque morphological characterization. Future studies should systematically evaluate the synergistic effect of multimodal imaging technology. (3) Methodologically, potential variability in manual segmentation may introduce variability in analysis, necessitating the development of automated segmentation models. (4) The classification of high-risk plaques relies on expert

neuroimaging consensus rather than histopathological validation, reflecting the inherent challenges of obtaining invasive gold standard validation in the intracranial vascular system. Although this approach is consistent with current clinical practice, the use of surgical specimens or autopsy analysis would strengthen diagnostic accuracy in subsequent studies.

In summary, by leveraging the integrated model of Habitat and ViT based on HR-VWI, we are able to deeply uncover the heterogeneous characteristics within plaque subregions and their intricate inter-subregional interactions. This integrated model markedly enhances the completeness and accuracy of image information, especially, it exhibits high precision in identifying plaques with high vulnerability. Its diagnostic accuracy has approached that of clinical specialists, and it offers significant additional value in predicting the risk of stroke recurrence, exhibiting notable incremental predictive benefits.

Contributors

GY and LZA designed and participated in all the experiments, HL, WZQ and ZXY evaluated the image processing and physician diagnostic abilities, ZQY, WJ, SYC, XBC followed up with patients and collected information, ZG, ZL and HTT conducted experiments on deep learning models, ZJH provided neurological advice, ZHL, ZG, ZL and LYD provided data from multiple centers, YRF provided HR-VWI advice, LYD provided epidemiological knowledge, CHK and ZJH contacted experts in relevant fields, coordinated all experimental planning, and provided financial support. All authors read and approved the final manuscript. All authors had full access to the data in the study and takes responsibility for the integrity of the data and the accuracy of the data analysis as well as the decision to submit for publication.

Data sharing statement

The data presented in this study are available on request from the first author. The code for radiomics, deep learning, and habitat radiomics analysis used in this study can be obtained from the https://github.com/Liziang12345/code-for-ecm.

Declaration of interests

The authors declare that they have no competing interests.

Acknowledgements

This study was supported by the National Natural Science Foundation of China (grant 82204933). Henan Key Laboratory of Neurorestoratology (HNSJXF-2021-004), 2019 Joint Construction Project of Henan Provincial Health Committee and Ministry of Health (SB201901061), and the Xin Xiang City Acute Ischemic Stroke Precision Prevention and Treatment Key Laboratory.

Appendix A. Supplementary data

Supplementary data related to this article can be found at https://doi.org/10.1016/j.eclinm.2025.103186.

References

1 Hou C, Lan J, Lin Y, et al. Chronic remote ischaemic conditioning in patients with symptomatic intracranial atherosclerotic stenosis (the rica trial): a multicentre, randomised, double-blind sham-controlled trial in China. *Lancet Neurol*. 2022;21:1089–1098.
2 Gutierrez J, Turan TN, Hoh BL, Chimowitz MI. Intracranial atherosclerotic stenosis: risk factors, diagnosis, and treatment. *Lancet Neurol*. 2022;21:355–368.
3 Lin Q, Liu X, Chen B, et al. Design of stroke imaging package study of intracranial atherosclerosis: a multicenter, prospective, cohort study. *Ann Transl Med*. 2020;8:13.
4 Kim J-M, Jung K-H, Sohn C-H, et al. Intracranial plaque enhancement from high resolution vessel wall magnetic resonance imaging predicts stroke recurrence. *Int J Stroke*. 2016;11:171–179.
5 Yang D, Liu J, Yao W, et al. The mri enhancement ratio and plaque steepness may be more accurate for predicting recurrent ischemic cerebrovascular events in patients with intracranial atherosclerosis. *Eur Radiol*. 2022;32:7004–7013.
6 Charles JH, Desai S, Jean Paul A, Hassan A. Multimodal imaging approach for the diagnosis of intracranial atherosclerotic disease (icad): basic principles, current and future perspectives. *Intervent Neuroradiol*. 2022;30:105–119.
7 Sui B, Gao P, Lin Y, Jing L, Qin H. Distribution and features of middle cerebral artery atherosclerotic plaques in symptomatic patients: a 3.0 t high-resolution mri study. *Neurol Res*. 2015;37:391–396.
8 Turan TN, Rumboldt Z, Granholm A-C, et al. Intracranial atherosclerosis: correlation between in-vivo 3t high resolution mri and pathology. *Atherosclerosis*. 2014;237:460–463.
9 Gillies RJ, Kinahan PE, Hricak H. Radiomics: images are more than pictures, they are data. *Radiology*. 2016;278:563–577.
10 Gatenby RA, Grove O, Gillies RJ. Quantitative imaging in cancer evolution and ecology. *Radiology*. 2013;269:8–14.
11 Wu J, Cao G, Sun X, et al. Intratumoral spatial heterogeneity at perfusion mr imaging predicts recurrence-free survival in locally advanced breast cancer treated with neoadjuvant chemotherapy. *Radiology*. 2018;288:26–35.
12 Hosny A, Parmar C, Quackenbush J, Schwartz LH, Aerts HJWL. Artificial intelligence in radiology. *Nat Rev Cancer*. 2018;18:500–510.
13 Pu Q, Xi Z, Yin S, Zhao Z, Zhao L. Advantages of transformer and its application for medical image segmentation: a survey. *Biomed Eng Online*. 2024;23.
14 Chen J, Frey EC, He Y, Segars WP, Li Y, Du Y. Transmorph: transformer for unsupervised medical image registration. *Med Image Anal*. 2022;82.
15 Chen C, Zhou K, Wang Z, Xiao R. Generative consistency for semi-supervised cerebrovascular segmentation from tof-mra. *IEEE Trans Med Imag*. 2023;42:346–353.
16 He S, Grant PE, Ou Y. Global-local transformer for brain age estimation. *IEEE Trans Med Imag*. 2022;41:213–224.
17 Cai H, Gao Y, Liu M. Graph transformer geometric learning of brain networks using multimodal mr images for brain age estimation. *IEEE Trans Med Imag*. 2023;42:456–466.
18 Park S, Araki M, Nakajima A, et al. Enhanced diagnosis of plaque erosion by deep learning in patients with acute coronary syndromes. *JACC Cardiovasc Interv*. 2022;15:2020–2031.
19 Wang Y, Zhao X, Liu L, et al. Prevalence and outcomes of symptomatic intracranial large artery stenoses and occlusions in China. *Stroke*. 2014;45:663–669.
20 Kopczak A, Schindler A, Sepp D, et al. Complicated carotid artery plaques and risk of recurrent ischemic stroke or tia. *J Am Coll Cardiol*. 2022;79:2189–2199.
21 Sun B, Wang L, Li X, et al. Intracranial atherosclerotic plaque characteristics and burden associated with recurrent acute stroke: a 3d quantitative vessel wall mri study. *Front Aging Neurosci*. 2021;13.
22 Hennerici MG. The unstable plaque. *Cerebrovasc Dis*. 2004;17:17–22.
23 Xia T, Zhao B, Li B, et al. Mri-based radiomics and deep learning in biological characteristics and prognosis of hepatocellular carcinoma: Opportunities and challenges. *J Magn Reson Imag*. 2023;59:767–783.
24 Li H, Liu J, Dong Z, et al. Identification of high-risk intracranial plaques with 3d high-resolution magnetic resonance imaging-based radiomics and machine learning. *J Neurol*. 2022;269:6494–6503.
25 O'Connor JPB, Rose CJ, Waterton JC, Carano RAD, Parker GJM, Jackson A. Imaging intratumor heterogeneity: role in therapy response, resistance, and clinical outcome. *Clin Cancer Res*. 2015;21:249–257.
26 Shi Z, Huang X, Cheng Z, et al. Mri-based quantification of intratumoral heterogeneity for predicting treatment response to neoadjuvant chemotherapy in breast cancer. *Radiology*. 2023;308.
27 Zhou H-Y, Guo J, Zhang Y, et al. Nnformer: volumetric medical image segmentation via a 3d transformer. *IEEE Trans Image Process*. 2023;32:4036–4045.
28 Liu Y, Nezami FR, Edelman ER. A transformer-based pyramid network for coronary calcified plaque segmentation in intravascular optical coherence tomography images. *Comput Med Imag Graph*. 2024;113.